ADVANCES IN FOREST FIRE RESEARCH

2022

Edited by
DOMINGOS XAVIER VIEGAS
LUÍS MÁRIO RIBEIRO

Pyrocumulonimbus Firepower Threshold: Selected learnings from the 'Black Summer' real-time trial.

Kevin Tory*; Mika Peace

Bureau of Meteorology. GPO Box 1289 Melbourne Vic Australia 3001,
{kevin.tory, mika.peace}@bom.gov.au

**Corresponding author*

Keywords

Pyrocumulonimbus, Fire-generated thunderstorms, Fire-weather prediction

Abstract

Pyrocumulonimbus (pyroCb) clouds are difficult to predict and can produce extreme and unexpected wildfire behavior that can be hazardous to fire crews. Many forecasters modify conventional thunderstorm diagnostics to predict pyroCb potential, by adding temperature and moisture increments to represent smoke plume thermodynamics near the expected plume condensation level. An alternative approach is to anticipate the minimum firepower required to generate pyroCb for a given atmospheric environment.This concept, termed the pyroCb firepower threshold (PFT), requires only atmospheric information, removing the need for subjective estimates of the fire contribution. A simple approach to calculating PFT was presented by Tory and Kepert (2021) that incorporates only basic plume-rise physics, and yields an analytic solution for the minimum heat flux required to enter the base of the plume for pyroCb to form. This version takes into consideration the magnitude of any inversion or stable layer the smoke plume must penetrate, the height the smoke plume must rise before sufficiently buoyant cumulus clouds form in the smoke plume, and it incorporates the impact of wind on plume rise via the Briggs plume-rise model. This PFT also offers important insight into plume behavior and pyroCb formation.

Many assumptions are made to close the equations and to maximise simplicity. Two of these assumptions are questioned in this paper following the investigation of two deep, moist pyro-convection cases that occurred during 'Black Summer' (southern Australia, September 2019—March 2020). The first assumption, consistent with many thunderstorm diagnostics, is that the moist (cloudy) plume is non-entraining, and the second assumption is that the plume is positively buoyant when it saturates and remains buoyant until it rises beyond the -20 ℃ level of the atmosphere. The first assumption underpredicts the fire-power required and the second assumption can overpredict the necessary firepower, since a vigorous plume may have sufficient kinetic energy to penetrate stable layers or capping inversions. Procedures are introduced to address these limitations.

1. Introduction

When intense smoke plumes develop on wildfires, the so-called plume-dominated fires, fire behaviour can become erratic, unpredictable and the fire ground can become highly dangerous for fire fighters. Strong updrafts can transport burning embers downwind, amplifying firespread through the ignition of spotfires ahead of the fire front. The formation of deep cumulus clouds with strong vertical motion in these plumes may amplify the dangerous fire behaviour, and introduce additional hazards separate to the fire such as extreme winds from evaporative downbursts, and tornadic-strength vortices. When conditions are favourable the fire-induced deep, moist convection can produce lightning with the potential to ignite more fires. These fire-generated thunderstorms (FGT) are also known as pyrocumulonimbus (pyroCb).

A procedure for identifying atmospheric conditions that favour deep, moist plume growth in wildfire smoke plumes, termed the Pyrocumulonimbus Firepower Threshold (PFT, Tory and Kepert 2021) was tested in a real-time trial (Tory 2020) during Australia's 'Black Summer' (southern Australia, September 2019—March 2020). The procedure estimates a theoretical minimum heat flux (or firepower) required for deep, moist plume growth. This version of the PFT (hereafter PFT1) takes into consideration the magnitude of any inversion or stable layer the smoke plume must penetrate, the height the smoke plume must rise before sufficiently buoyant cumulus clouds form in the smoke plume, and it incorporates the impact of wind on plume rise via the Briggs plume-rise model (e.g., Briggs 1984). Below the condensation height it is assumed that the smoke plume can be described

by a Briggs plume rising through a neutrally stable layer of constant background wind. Above the condensation height, it is assumed the rising moist plume can be described by simple parcel theory (non-entraining, as applied to common thunderstorm forecast products such as Convective Available Potential Energy, CAPE).

During the real-time trial PFT1 forecast maps provided excellent guidance for predicting deep, moist pyro-convection (hereafter DMPC). A selection of interesting DMPC cases were investigated in detail, using a manual PFT1 analysis method applied to thermodynamic diagrams, yielding important insight into plume behaviour, which has inspired further development and tuning of PFT products. In this short paper, two such cases are presented.

2. PFT

The full PFT1 derivation is provided in Tory and Kepert (2021), as well as an approximated form designed for estimating and visualising PFT1 manually on a thermodynamic diagram,

$$PFT1 \sim 0.3 \times \left(z_{fc}\right)^2 \times U \times \Delta\theta_{fc}. \qquad 1.$$

Here z_{fc} is the free-convection height in units of km (the minimum height the plume must rise to initiate deep moist pyro-convection), U is the average velocity magnitude of the mixed layer horizontal wind, units ms^{-1}, and $\Delta\theta_{fc}$ represents how much warmer the plume needs to be than the mixed-layer potential temperature, units ℃ (or K). These units yield PFT1 in GW. An example from the evening of the disastrous Black Saturday fires of 2009 is shown in Fig. 1. The mixed-layer potential temperature (thick red line) and specific humidity (thick cyan line) represent the average thermodynamic properties of air entrained into the plume. The saturation point curve is approximated by a straight line representing a 15:1 ratio of temperature to moisture increments (units $K/g\ kg^{-1}$, blue line) produced by the fire (Luderer et al. 2009, Tory et al. 2018). It represents a range of possible positions on the diagram where the plume can reach saturation. The minimum-buoyancy plume-path that freely convects to a level cooler than -20 ℃ is indicated by the gold curve. The free-convection height (z_{fc}) is the height at the base of the gold curve. Here the plume must be at least $\Delta\theta_{fc}$ warmer than the mixed-layer potential temperature (thick red line), and the average mixed-layer wind, U, can be estimated from the wind barbs highlighted in green.

In theory, the fire must be able to produce enough firepower for the plume to rise to at least a height of z_{fc}, while maintaining an average plume temperature of at least $\Delta\theta_{fc}$ warmer than the mixed-layer potential temperature, while battling the wind, U, which inhibits the plume rise by stretching the plume out downwind and exposing it to more dilution from entrainment.

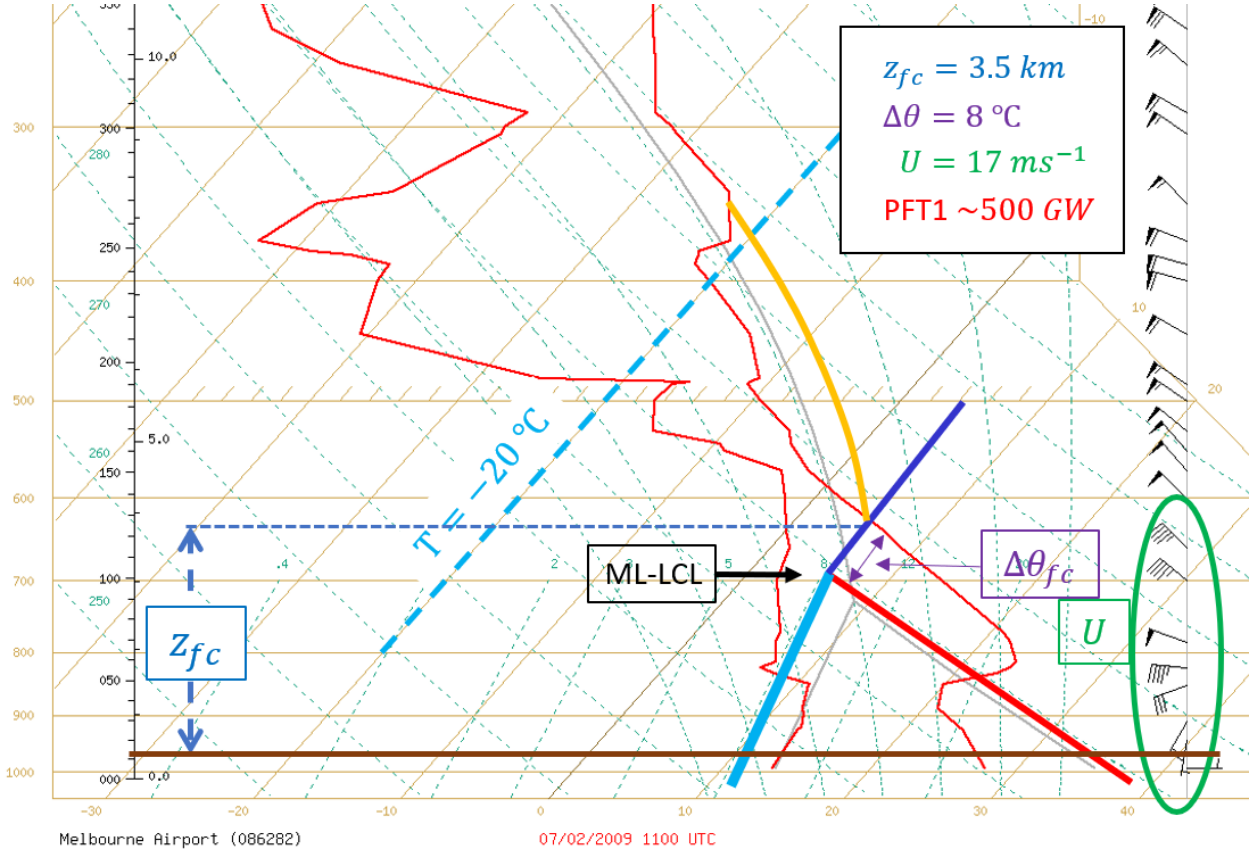

Figure 1- Melbourne Airport sounding 1100 UTC, 7 February 2009 (10 PM local time), with markers used in the manual PFT calculation (Eq. 1). Thick red and cyan lines represent the mixed-layer potential temperature and specific humidity respectively, with the mixed-layer lifting condensation level (ML-LCL) marked at the apex of these two lines. The saturation point (SP) curve (approximated by the blue line) identifies the potential plume condensation positions. The minimum-buoyancy plume-path is indicated by the gold curve. The free-convection height (z_{fc}) is the height at the base of the gold curve. The plume must be at least $\Delta\theta_{fc}$ warmer than the mixed-layer potential temperature (thick red line), and the average mixed-layer wind term (U) can be estimated from the wind barbs highlighted in green.

3. Case study events

One focus of forecasters during the trial was the prediction of lightning in DMPC because lightning is generally well observed and offers a clear distinction between towering pyrocumulus and pyrocumulonimbus clouds. Cloud-top temperature (CTT) observations from satellites are readily available that enable near-real-time assessment of DMPC maturity, and an indication of when the convection has penetrated the typical charge separation layer (-15 to -25 ℃) above which lightning might be expected to develop. However, it was common for DMPC to develop with CTT much cooler than -25 ℃ without lightning. Then on Sunday 2 Feb 2020 forecasters were confounded by lightning that developed in DMPC when the CTT only reached -15 ℃. This was unexpected, especially given that on the previous day DMPC with CTT of -45 ℃ developed on a fire nearby, with no lightning.

To try and understand these differences, a PFT1 analysis was performed for each case, with both identifying scenarios where assumptions used to simplify PFT1 need to be reconsidered. The first of these simplifying assumptions is that a rising plume-parcel is always buoyant, i.e., it is assumed a parcel cannot penetrate a capping inversion unless it is warmer than that inversion. The second simplifying assumption is that the moist plume is non-entraining, i.e., it does not lose buoyancy from dilution and cloud moisture evaporation when cooler drier air is mixed into the plume from outside.

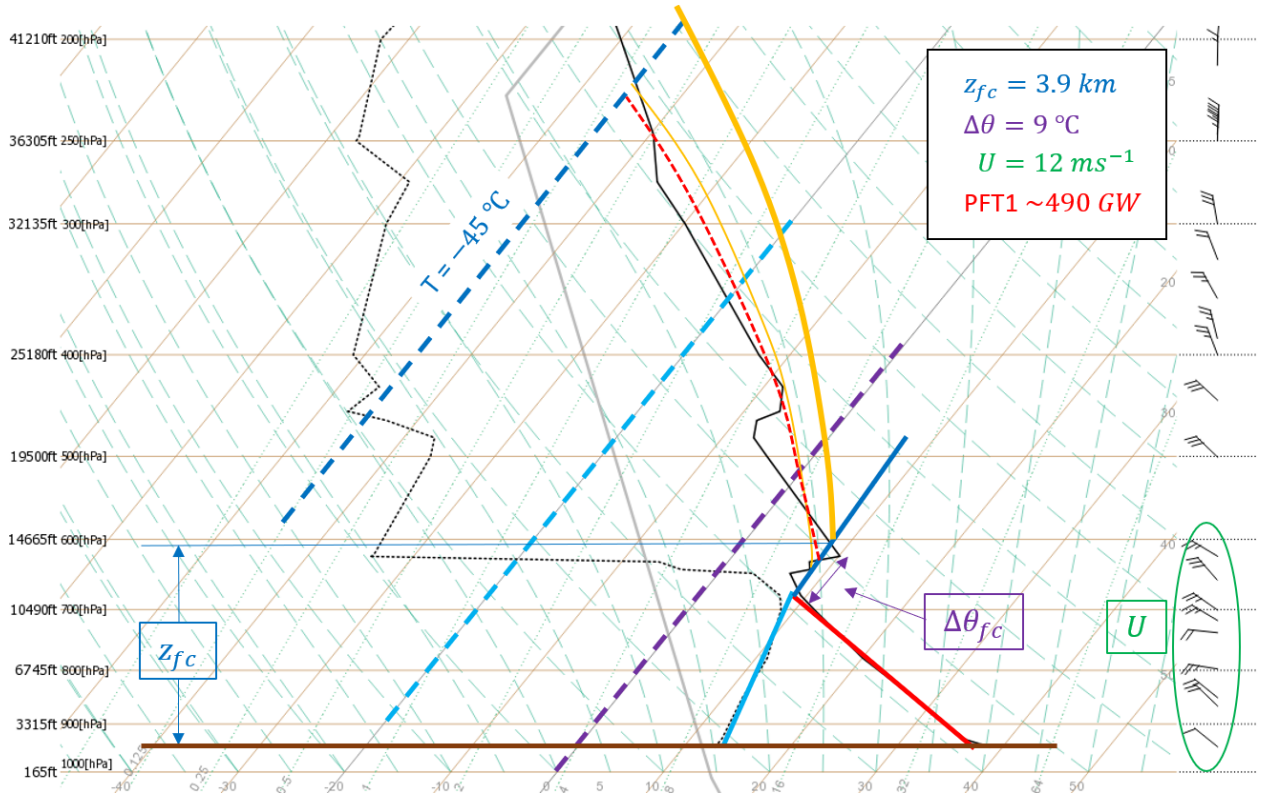

Figure 2- Canberra sounding 1 PM local time (0200 UTC) Saturday 1 Feb. The solid and dotted black lines represent temperature and dewpoint temperature respectively. The 0, -20 and -45 ℃ temperature lines are indicated by purple, cyan and blue dashed lines respectively. The solid red and cyan lines show a mixed layer temperature and dewpoint temperature of constant potential temperature and specific humidity that represent the average quantities entrained into a hypothetical plume rising through the mixed layer. The solid blue line is an approximate Saturation Point curve. The gold lines are moist parcel paths emerging from the SP curve, one with minimum buoyancy just able to breach the capping inversion and exceed the -20 ℃ level (thick, used in PFT1), and the other (thin) represents a non-entraining parcel path corresponding to the observed cloud-top temperature of -45 ℃. The red dashed line is a hypothetical parcel path that reaches the observed cloud top temperature with some overshooting, takes into account buoyancy losses associated with entrainment, and assumes sufficient vertical kinetic energy to penetrate the lower temperature inversion (between 650 and 610 hPa). The three ingredients for a manual PFT1 calculation are illustrated, and their estimated values shown in the legend.

The PFT1 analyses used to explore the two events are presented in Figs 2 and 3 respectively. Dark blue dashed lines corresponding to the observed CTT, and corresponding non-entraining moist-plume parcel paths (thin gold lines) have been added to highlight the discrepancy between the observed, and minimum-predicted equilibrium levels. On both days the minimum-predicted equilibrium level (top of the thick gold line) is much colder (-60 ℃ and -50 ℃ respectively) than the observed CTTs (-45 ℃ and -15 ℃ respectively). However, the zero-entrainment parcel paths matching the observed CTTs (thin gold lines) both have regions of negative buoyancy, which is counter to the PFT1 assumption of positive buoyancy everywhere.

In the first case (Fig. 2), negative buoyancy is encountered when the thin gold line penetrates the capping inversion near 600 hPa, and it also approaches zero buoyancy near 450 hPa. If this parcel path is realistic, it implies that the plume had sufficient kinetic energy to penetrate the capping inversion.

A theoretical kinetic energy can be calculated from the Briggs plume-rise equations, which, with a few simplifications (not shown), becomes,

$$E_k \sim 4.3 \times \Delta\theta_{SP} \times z_{SP}. \qquad 2.$$

Here E_k is the vertical kinetic energy of a plume parcel in units of Jkg^{-1}, the subscript SP refers to a point on the SP curve (blue solid line), and $\Delta\theta_{SP}$ and z_{SP} are analogous to $\Delta\theta_{fc}$ and z_{fc} (same units). Importantly, Eq. 2 shows that the larger $\Delta\theta_{SP}$ and z_{SP}, the larger the plume kinetic energy.

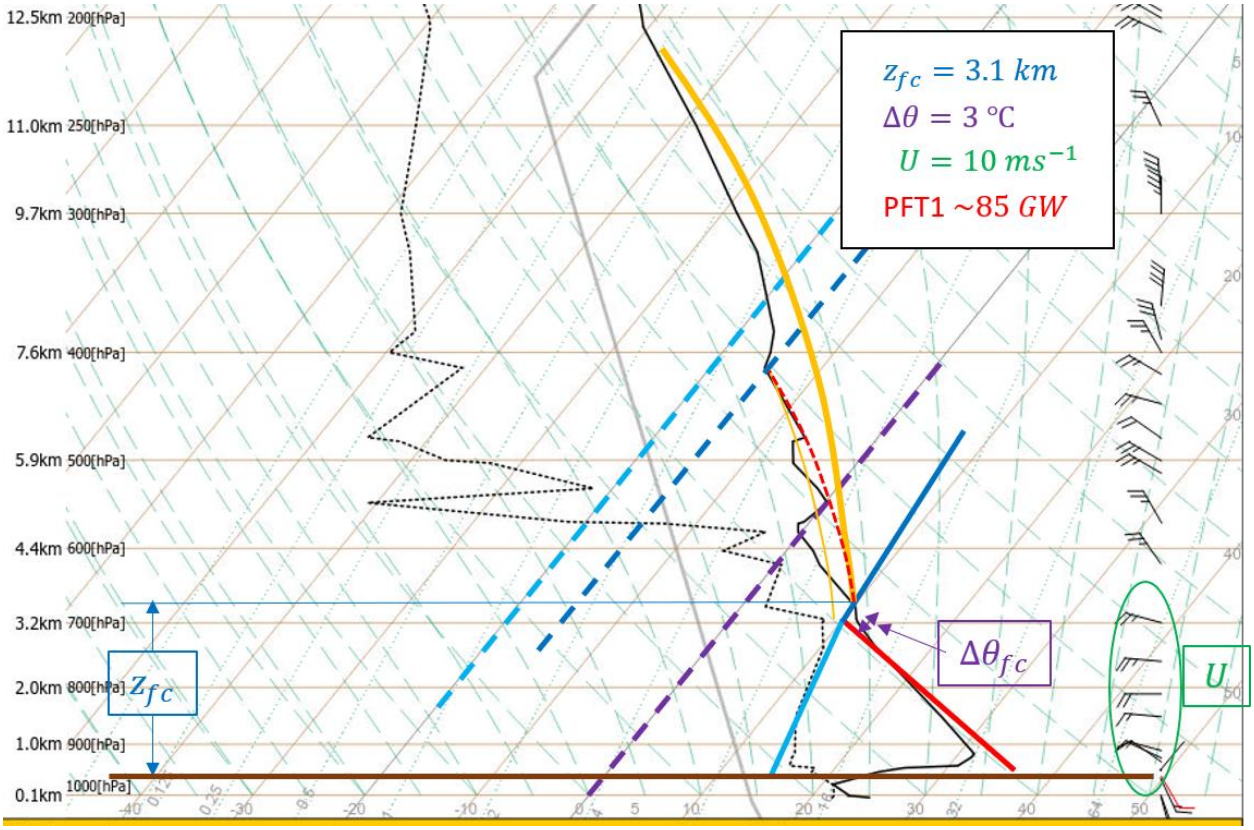

Figure 2- As in Fig. 2 but for the Sydney sounding 2 PM local time (0300 UTC) Sunday 2 Feb. Observations from a PAWS (RF55) located at Faulconbridge (elevation 410m, 20 km north of the fire) were used to estimate the actual conditions below 1.0 km.

In the second case (Fig. 3), the negative buoyancy regions encountered by a parcel on the thin gold line are more substantial than the first case. These include a stable layer just above the ML-LCL and two inversions near 550 and 470 hPa. Furthermore, the corresponding $\Delta\theta_{SP}$ would be close to zero or even negative, suggesting any plume elements at the base of the thin yellow line would not only have negative buoyancy, but no vertical kinetic energy prior to plume condensation. It follows that the real plume parcel paths must have had $\Delta\theta_{SP} \geq 2$ to have reached the observed CTT (assuming the temperature trace represents the fire environment), which implies they would have had vertical momentum at saturation, and were probably buoyant too. However, any non-entraining parcel paths (moist adiabats) matching these $\Delta\theta_{SP}$ values would rise well beyond the observed CTT levels. It follows that any plume parcel with $\Delta\theta_{SP} \geq 2$ that reaches equilibrium at -15 ℃ must have lost buoyancy while ascending. The most likely cause of buoyancy loss is entrainment of cooler and drier air. The warmer plume is diluted by the cooler entrained air, and the evaporation of cloud water by the entrained dry air further cools the plume.

Hypothetical entraining-plume paths, are included in Figs 2 and 3 (red dashed lines). Entrainment is often expressed as a dilution fraction per km of ascent. While the entraining interface between the plume and environment is more turbulent in rapidly rising plumes (which enhances entrainment), plume elements spend less time ascending and hence less time entraining, with the net effect that rapidly rising plumes experience less total entrainment than slower rising plumes (e.g., Gregory 2001). It follows that as a general rule, larger (smaller) $\Delta\theta_{SP}$ would relate to greater (smaller) ascent rates and thus smaller (larger) entrainment rates.

On both days very dry air was located above about 600 hPa, indicating entrainment would be particularly detrimental to plume buoyancy. However, the $\Delta\theta_{SP}$ values corresponding to the hypothetical entraining plume paths (difference in potential temperature between the SP and mixed-layer value) are about 7 ℃ (Fig. 2) and 3 ℃ (Fig. 3) respectively, suggesting the former would have ascended more rapidly and thus experienced less entrainment than the latter. Furthermore, it suggests entrainment may only be significant for cases with relatively small $\Delta\theta_{SP}$.

4. Summary and Discussion

The two cases presented suggest the PFT1 assumptions of non-entraining moist plume paths that are everywhere buoyant from condensation to the -20 ℃ isotherm (thick gold lines in Figs 2 and 3), may not always be reasonable. Plumes with non-trivial $\Delta\theta_{SP}$ are likely to have sufficient vertical kinetic energy to penetrate some stable layers and inversions, and plumes with smaller $\Delta\theta_{SP}$ will likely experience greater buoyancy losses from entrainment. However, the associated errors from ignoring these effects will partly cancel, since the plume-kinetic-energy omission yields a PFT1 over-prediction and the entrainment omission yields a PFT1 under-prediction.

A manual procedure for estimating the minimum $\Delta\theta_{SP}$ of a plume capable of penetrating a stable layer is under development. The plume kinetic energy is estimated using Eq. 2, and the integrated buoyancy force it will encounter is estimated from the area between the parcel path and the environment temperature trace, similar to the calculation of convective inhibition (CIN) used in CAPE calculations. Where the E_k and CIN balance, the plume is deemed to just have sufficient kinetic energy to penetrate the stable layer. Estimating entrainment rates is considerably more complex. It may be necessary to add 1—3 ℃ to $\Delta\theta_{SP}$ to account for buoyancy losses due to entrainment, with a larger increment added if the initial $\Delta\theta_{SP}$ is relatively small and a smaller increment if it is relatively large (suitable increments are yet to be determined). Finally, the updated $\Delta\theta_{SP}$ along with a matching z_{SP} can be fed into Eq. 1 to calculate an improved PFT. There will be many cases in which these modifications will have no or negligible impact on the PFT result. It is anticipated that users will soon identify environments in which taking these additional steps will yield improved PFT estimates.

5. Acknowledgements

Thanks to Zach Porter and David Wilke for providing soundings and plume-behaviour descriptions for the Bees Nest, Orroral/Clear Range and Erskine Creek fires.

6. References

Briggs, G. A., 1984: Plume rise and buoyancy effects. Atmospheric Science and Power Production, D. Randerson, Ed., U.S. Dept. of Energy DOE/TIC-27601, available from NTIS as DE84005177, 327—366.

Gregory, D., 2001: Estimation of entrainment rate in simple models of convective clouds. Quart. J. Roy. Meteor. Soc., 127, 53—72, https://doi.org/10.1002/qj.49712757104.

Luderer, G., J. Trentmann and M. O. Andreae, 2009: A new look at the role of fire released moisture on the dynamics of atmospheric pyro-convection. Int. J. Wild. Fire, 18, 554—562.

Tory, K. J., W. Thurston and J. D. Kepert, 2018: Thermodynamics of pyrocumulus: A conceptual study. Mon. Wea. Rev., 146, 2579—2598. DOI: 10.1175/MWR-D-17-0377.1

Tory, K. J., 2020: The real-time trial of the pyrocumulonimbus firepower threshold. Southern Australia 2019/2020 fire season. https://www.bnhcrc.com.au/sites/default/files/managed/downloads/the_real-time_trial_of_the_pyrocumulonimbus_firepower_threshold_0.pdf

Tory, K. J., and J. D. Kepert, 2021: Pyrocumulonimbus Firepower Threshold: Assessing the atmospheric potential for pyroCb. Weather and Forecasting, 36, 439—456. https://doi.org/10.1175/WAF-D-20-0027.1